HHS Public Access

Author manuscript

Nat Methods. Author manuscript; available in PMC 2016 July 01.

Published in final edited form as:

Nat Methods. 2016 January ; 13(1): 59–62. doi:10.1038/nmeth.3667.

Concentric-Flow Electrokinetic Injector Enables Serial Crystallography of Ribosome and Photosystem-II

Raymond G. Sierra[1,*], **Cornelius Gati**[2], **Hartawan Laksmono**[1], **E. Han Dao**[1], **Sheraz Gul**[3], **Franklin Fuller**[3], **Jan Kern**[3,4], **Ruchira Chatterjee**[3], **Mohamed Ibrahim**[5], **Aaron S. Brewster**[3], **Iris D. Young**[3], **Tara Michels-Clark**[3], **Andrew Aquila**[4], **Mengning Liang**[4], **Mark S. Hunter**[4], **Jason E. Koglin**[4], **Sébastien Boutet**[4], **Elia A. Junco**[4], **Brandon Hayes**[4], **Michael J. Bogan**[1], **Christina Y. Hampton**[1], **Elisabetta V. Puglisi**[6], **Nicholas K. Sauter**[3], **Claudiu A. Stan**[1], **Athina Zouni**[5], **Junko Yano**[3], **Vittal K. Yachandra**[3], **S. Michael Soltis**[7], **Joseph D. Puglisi**[6], and **Hasan DeMirci**[1,7,*]

[1]Stanford PULSE Institute, SLAC National Accelerator Laboratory, Menlo Park, CA, USA

[2]Center for Free-Electron Laser Science, Deutsches Elektronen-Synchrotron, Hamburg, Germany

[3]Lawrence Berkeley National Laboratory, Berkeley, CA, USA

[4]Linac Coherent Light Source, SLAC National Accelerator Laboratory, Menlo Park, CA, USA

[5]Institute für Biologie, Humboldt University of Berlin, Berlin, Germany

[6]Department of Structural Biology, Stanford University School of Medicine, Stanford, CA, USA

[7]Stanford Synchrotron Radiation Lightsource, SLAC National Accelerator Laboratory, Menlo Park, CA, USA

Abstract

In this work, a concentric-flow electrokinetic injector delivered microcrystals of *Geobacillus stearothermophilus* thermolysin (2.2 Å structure), *Thermosynechococcus elongatus* photosystem II (< 3 Å diffraction) and *Thermus thermophilus* small ribosomal subunit (3.4 Å structure). The first ambient-temperature X-ray crystal structure of the 30S subunit bound to the antibiotic paromomycin was obtained in its native mother liquor. Compared to previous cryo-cooled structures, this new structure showed that paromomycin binds to the decoding center in a different conformation.

[*]Correspondence should be addressed to H. DeMirci (; Email: Hasan_DeMirci@Stanford.edu) or R. G. Sierra (; Email: rsierra@stanford.edu)

AUTHOR CONTRIBUTIONS

HD and RGS designed and coordinated the project. RGS, HL, HD, CAS, CYH, SG, FF and MJB developed the coMESH injection method. CG executed the ribosome data reduction. Ribosome and thermolysin structures were refined by HD. NKS, ASB, IDY, and TMC processed PSII and thermolysin diffraction data. Samples were prepared by HD, EHD, BH, RC, IDY, MI, JK and AZ. The experiment was executed by RGS, HD, HL, CAS, EHD, SG, FF, JK, RC, MI, ML, MH, JEK, SB, EAJ, JY, and VKY. Data were analyzed by HD, CG, RGS, EVP, JK, JY, VKY, SMS, JDP. The manuscript was prepared by HD, RGS, EHD, CG, HL, CAS, and JK with input from all the coauthors.

COMPETING FINANCIAL INTERESTS

The authors declare no competing financial interests.

Keywords

SFX; ribosome; photosystem II; electrospinning; concentric-flow; antibiotic; ambient temperature crystallography

Introduction

The development of serial femtosecond X-ray crystallography (SFX)[1] at X-ray free electron lasers (XFELs) pushes the frontiers of structural biology[2, 3]. In addition to pursuing structures of new targets, SFX can be used at ambient temperature to re-examine structures of biological macromolecules and complexes previously obtained at cryogenic temperatures[4].

Methods for SFX are usually validated using protein crystal standards[5, 6]. Success with these standards does not translate directly to more difficult systems, such as ribosomes and photosystem II (PSII). For SFX, the ideal injection method minimally alters the crystals' growth medium (mother liquor), consumes minimal sample and maximizes the hit rate. Liquid injectors currently offer the best hit rates by using the full repetition rate of the XFELs compared to current fixed-target approaches[7], but have drawbacks. The gas dynamic virtual nozzle (GDVN)[8] focuses a liquid jet with a gas stream and provides robust sample delivery, but consumes samples inefficiently as a large volume of sample flows unused between XFEL pulses and is generally incompatible with high-viscosity media. The microfluidic electrokinetic sample holder (MESH)[9] operates at lower flow rates by applying voltage rather than pressure. While operation of the MESH at atmospheric conditions is trivial, the low vacuum pressures of existing XFEL experiment chambers cause the fluid at the meniscus to evaporate quickly. Consequently, freezing and precipitation of solutes occurs, causing jet failures and preventing data collection. A typical workaround is to place an additive in the crystallization sample. The lipidic cubic phase (LCP)[10] and grease-matrix injectors[11] are more efficient due to their high-viscosity carrier media, which enables a slow extrusion of the samples; however, the medium itself has high background scattering and must also be compatible with the crystals. The SFX field still requires more robust injection methods for delivering soluble protein crystals in their native mother liquor with minimal sample consumption. The concentric MESH (coMESH) injection method described below addresses these issues.

The coMESH uses an inner capillary to introduce crystalline samples, suspended in their native mother liquor, into the XFEL beam. An outer sheath (the "sister liquor") prevents dehydration and freezing of the sample fluid upon introduction to the vacuum chamber (Fig. 1; Supplementary Figs. 1 and 2). This concentric-flow design improves upon the prior MESH method and solves its previous limitations (Supplementary Table 1). The coMESH improved the hit rate and the quality of data collected from PSII crystals over the single-capillary MESH (Supplementary Figs. 3b,c; 4a,b; and 5). This low flow method enabled collection of the first complete, ambient temperature, 3.4 Å dataset of *T. thermophilus* 30S ribosomal subunit bound to the antibiotic paromomycin.

Results

Improved PSII data collection with the coMESH

The crystallization condition of PSII crystals contained a high percentage of PEG 5,000[12], which caused the meniscus of the MESH to dehydrate quickly in vacuum. Large deposits of dried PEG 5,000 accumulated at the tip of the injector and caused frequent jet failures, limiting the data collection time between blockages (Supplementary Fig. 4c). Use of the coMESH with co-terminal capillaries eliminated freezing and drying issues and allowed the observation of diffraction beyond 3.0 Å (Supplementary Fig. 5b) at the Coherent X-ray Imaging (CXI) instrument of LCLS[13]. Using the coMESH permitted continuous data collection for 2–2.5 hours, an improvement over mean data collection times of 20–30 minutes between failures of the jet in the single-capillary MESH setup due to the PEG buildup.

Ambient temperature 30S ribosomal subunit structure

In a separate protein crystal screening (PCS) beamtime, the structure of a 30S-paromomycin complex was determined to 3.4 Å at ambient temperature by SFX using coMESH sample delivery at the CXI instrument[13] (details summarized in Supplementary Table 2). Substantial conformational shifts were observed (Fig. 2) when the ambient-temperature structure was compared with a cryo-cooled synchrotron structure (3.35 Å, PDB accession code 4DR2)[14]. Superposition of the cryo-cooled and ambient-temperature structures showed that the *head* and *beak* domains adopt slightly altered conformations (Fig. 2). A least-squares alignment of all 17,056 16S rRNA atoms in the two 30S structures showed an overall RMSD of 0.488 Å. Interesting conformational differences (up to 3.6 Å) between the two structures were found at the 926–934 and 1,378–1,385 regions that are part of helix 28 (h28) of the 16S rRNA (Fig. 3a,b). Comparison of the two structures also revealed differences within the H-bond network of paromomycin (Fig. 3d). In the cryo-cooled structure, the O23 atom of paromomycin engaged in a 2.85 Å H-bond with the N4 atom of the m5C1407 residue compared to 3.4 Å at ambient temperature, suggesting a weakening of this particular interaction. Also, a 1.4 Å shift in the position of O23 introduced further changes in the conformation of paromomycin ring III (Supplementary Table 3). For example, in the new state, O23 protrudes out of the experimental F_o–F_c simple difference omit map (Fig. 3c).

Discussion

The coMESH leverages the low flow capabilities of the electrokinetic injector[9] and allows injection of protein solutions and microcrystals in their unperturbed native buffers and mother liquors respectively. The ability to use 100 μm inner diameter (ID) capillaries allows unfiltered crystals up to 40 μm in size to flow without clogging, compared to the typical 40–75 μm ID capillaries used in other setups, while keeping flow rates typically between 1–3 μl/min. LCP injection[10] flows at hundreds of nanoliters per minute but requires the sample to either grow or be mixed into the viscous LCP. For membrane proteins like GPCRs, LCP injection is an ideal technique; however, it is unclear if other soluble proteins can grow or be mixed into the LCP matrix easily. Greases, oils, and gels, for example, can be ideal for certain crystals but not others[11]. The coMESH permits protein crystals to flow in their

established mother liquor and co-flow with an appropriate sister liquor (Supplementary Table 1).

A key limitation of the prior single-capillary approach was the need to dope the mother liquor such that the final crystal suspension would not freeze *in vacuo*. Finding an additive that enables sample injection while maintaining the integrity of the crystals is not always feasible. In the coMESH, however, both capillaries are placed co-terminally such that the sister liquor protects the mother liquor from vacuum effects with minimal mixing prior to reaching the incident XFEL probe[15] (Fig. 1). The prevention of freezing, dehydration and precipitation of the sample slurry *in vacuo* maximizes the time available for data collection. Alteration of the mother liquor is also obviated. A 2.2 Å structure of thermolysin (Supplementary Fig. 6) was collected with the coMESH in an alternate configuration (Supplementary Fig. 3d). The coMESH improved the data collection from both the crystalline and the solution samples of PSII. The increase in mean run-time between blockages by a factor of five, compared to the previous single-capillary MESH, permitted more efficient use of scarce beamtime by injecting the high-concentration PEG 5,000 mother liquor of the PSII crystals without drying issues.

In a previous PCS time, SFX data for 30S ribosomal subunit crystals were collected at the CXI instrument[16] using GDVN injection; the crystals diffracted to 5.5 Å. In those data, 637 indexed hits were identified out of 1,074,902 diffraction patterns. More than 15 ml of sample was used during the six hour beamtime. In comparison, 20,667 indexed hits were identified out of 44,106 patterns collected from 360 μl of sample consumed in 2 hours of data collection to solve the 3.4 Å structure reported here.

Ribosomes are structurally dynamic and undergo local and large-scale conformational rearrangements during the individual steps of protein synthesis[17]. X-ray crystallography data for ribosomes and other large complexes are typically collected at cryogenic temperatures as these crystals are extremely sensitive to radiation damage[18]. Cryo-cooling enables data collection but may mask useful details about local and global conformational dynamics and allostery. Structures of ribosomes obtained at temperatures closer to the physiological range, can reveal alternative conformations and structural dynamics, such as the alternative conformation of h28 (hinge 1) identified here. Some of these structural variations may be precisely linked to function[19]. Hinge 1 of the 30S subunit[19] confers the remarkable plasticity of the head domain and allows the head of the ribosome to move freely between functional states during translation. Here the h28 phosphate backbone exhibits up to 3.6 Å shifts at ambient temperature (Figs. 2b and 3b), compared to the more rigidified and dehydrated cryo-cooled structure. These differences can have large implications for understanding the binding of paromomycin to the ribosome and the effects of antibiotics binding to ribosomes in general. The same motivation may also hold for many other enzymatic systems such as PSII, a membrane metalloprotein complex that so far has been studied at high resolution only in cryogenically trapped states[20] yet functions at ambient temperatures.

Conclusions

A concentric-flow liquid injection technique for SFX was demonstrated. The outer fluid, a compatible sister liquor, protected the sample-carrying inner liquid line from the evaporative

effects of vacuum, and allowed crystals of large soluble complexes—in their native mother liquor—as well as standards, to be delivered for SFX studies *in vacuo*. The coMESH allows a wider range of soluble protein crystal slurries to be used in SFX. The sister liquor addresses the MESH's inability to tolerate vacuum injection without using an appropriately modified mother liquor that maintains the integrity of the suspended crystals. The off-the-shelf parts of the coMESH, along with the unperturbed mother-liquor, brings SFX experiments to a wider community that demands low sample consumption and whose crystals cannot be transferred to different crystallization conditions, such as adding glycerol, grease, or LCP. PSII and 30S ribosomal subunit crystals were delivered in their native mother liquors with reduced injection failure while minimizing sample consumption. At ambient temperature, the 30S crystals diffracted to a resolution similar to that at a synchrotron, and differences were observed between the new XFEL structure and the previous cryo-cooled structure. This new information provides a more comprehensive and accurate model of ribosome–antibiotic interactions near physiological temperatures and accelerates structure-based drug design for new-generation antibiotics targeting bacterial ribosomes.

The coMESH arrives at an exciting time in the structural biology community where cryo-EM and cryo-crystallography structures of complexes can be combined with SFX to study biological macromolecules at near-physiological temperatures. In the future, the concentric geometry of the coMESH could easily be modified to recess the inner capillary and create the basis of a mixing apparatus to explore structural intermediates over time[15]. The sister liquor could be doped with a reactant to initiate structural changes for time-resolved mix-and-probe experiments at XFELs, such as mixing of ribosomes with antibiotics, substrates and translation factors. Time-resolved SFX could move beyond photo-excited systems to include a vast mix-probe regime. These future mix-probe studies would allow examination of the dynamic details of binding events on hitherto-inaccessible timescales, temperatures and resolution.

METHODS

Methods and any associated references are available in the online version of the paper.

Accession codes

Protein Data Bank: Coordinates and structure factors of 30S-Paromomycin complex and thermolysin have been deposited under accession codes 5BR8 and 5DLH respectively.

Note: Any Supplementary Information and Source Data files are available in the online version of the paper.

ONLINE METHODS

Preparation and Crystallization of 30S Ribosomal Subunits

30S ribosomal subunits from *T. thermophilus* HB8 (ATCC27634)[21] were prepared as previously described[22, 23]. Purified 30S ribosomal subunits were crystallized at 4 °C by the hanging drop method using a mother liquor solution containing 17% (v/v) 2-methyl-2,4-

pentanediol (MPD), 15 mM magnesium acetate, 200 mM potassium acetate, 75 mM ammonium acetate and 100 mM 2-(*N*-morpholino) ethanesulfonic acid (MES)-KOH (pH 6.5). Microcrystals 3–10 × 3–10 × 20–30 μm^3 in size were harvested in the same mother liquor composition, pooled (total volume of 800 μl loaded) and supplemented with 80 μM paromomycin for 48 hours before data collection. Crystal concentration was approximated to be 10^{10}–10^{11} particles per ml based on light microscopy and nanoparticle tracking analysis (NanoSight LM10-HS with corresponding Nanoparticle Tracking Analysis (NTA) software suite (Malvern Instruments, Malvern, UK).

Preparation and Crystallization of PSII Crystals and Solution

Crystals of *T. elongatus* PSII were grown as described previously[12]; a uniform crystal size of 5–15 μm was achieved using a seeding protocol[24]. The crystals were transferred to a final buffer of 35% (w/v) PEG 5,000, 0.1 M ammonium sulfate, 0.1 M TRIS (pH 7.5), before loading them into a 250 μl volume Hamilton Gastight syringe for sample injection. PSII solution samples were prepared from purified dimeric PSII, following the procedure described previously[25]. The final solution was adjusted to a protein concentration of ~6.7 mM chlorophyll (70 mg/ml protein), glycerol content of 40% (v/v) and a detergent (β-dodecyl maltoside) concentration of 0.015% (v/v).

Preparation of thermolysin crystals

Lyophilized thermolysin from *G. stearothermophilus*, purchased from Hampton Research (La Jolla, CA, USA), was resuspended in 0.05 M NaOH at a concentration of 25 mg/ml. and crystallized as described previously[11,15] using PEG 2,000 as precipitant. Crystals had average dimensions of 3 μm × 5 μm and were transferred in a final buffer of 10% (w/v) PEG 2,000, 38% (v/v) glycerol, 5 mM $CaCl_2$, 100 mM MES, pH6.5, before injection.

Operating the coMESH

Before connecting the central sample line, the sister liquor was loaded, flowed and electrically focused. Once a slightly stable jet was achieved, the central sample line was connected. Notably, the sister liquor never fully stabilized because of the entrained air from the disconnected sample line continuously introducing bubbles. The central sample line had much less fluidic resistance compared to the outer line; connecting it first with a vacuum sensitive sample will cause immediate jet clogging and blockages; like the helium sheath line of the GDVN, the outer line should always be on while operating in vacuum. The sister liquor was set to flow at, or near, the flow rate of the mother liquor. If diffraction hits were not being observed, the sister liquor flow was reduced and/or the mother liquor flow was increased slowly to ensure the jetting remains stable, and until the diffraction patterns appear; it is possible that the sister liquor flow rate was too high compared to the mother liquor and was pinching off the inner flow of crystals.

Selecting a sister liquor

The main goal of the sister liquor is to survive the vacuous environment (10^{-5} Torr) and protect the inner sample line from the adverse vacuum effects. In the case of the co-terminal coMESH, the compatibility between the sister liquor and the protein crystals was not

considered since the fluid interaction occurred just before the sample is probed, allowing minimal time, if any, for the fluids to mix. The limiting constraint is typically the availability of the fluid and its viscosity. For simplicity, the MPD-containing sister liquor described in Supplementary Table 1 seems to be an ideal starting choice. The buffer has proven to be quite reliable and survives the vacuum injection with minimal issues of leaving behind dried sucrose, or allowing precipitate such as salt or PEG to stay adhered to the capillary tip. The lower viscosity allows the sister liquor to be pumped easily by a standard syringe pump through the more resistive *cross* manifold or concentric annular flow before the exit region of the capillary. Using a more viscous sister liquor, such as the glycerol- 2,000 mixture in Supplementary Table 1 for example, can aid the mother liquor in certain instances, but may not flow fast enough to keep the mother liquor sufficiently quenched. Although this mixture worked to inject water (a difficult mother liquor to deliver at low flow rates due to its near-instantaneous freezing when introduced to vacuum), it was easy for slight perturbations in the flow rates to cause the sample line to be exposed to vacuum and freeze. The high viscosity of the glycerol and PEG solution compared to the MPD solution made it difficult to increase the flowrate to ensure protection.

If MPD is not viable, the crystal's known cryo-protectant solution from standard synchrotron studies is another possibility. Oils may not be ideal for vacuum injection or sister liquor, as outgassing of the oil may not be tolerable by the sensitive in-vacuum optics in the experiment. More importantly, the oil will likely limit the charging ability of the sister liquor, which will hinder the focusing of the liquid jet. The novelty of the sister liquor is that properties of the fluid can be modified with minimal concern for the integrity of the crystal in the central line. For example, if a mother liquor with high-molarity salt is causing rapid dehydration in vacuum and the formation of data-compromising salt crystals, the sister liquor can be formulated with reduced salt concentration to hundreds of millimolar, some cryo-protectant and pH buffer to aid the injection with the coMESH.

If a high viscosity sister liquor is required, but cannot easily flow fast enough to protect the mother liquor, then changes to the coMESH capillaries can be made, such as shortening lengths and increasing diameters where possible. Also, instead of a syringe pump, an HPLC or a high pressure reservoir can be employed. In this current design, the off-the-shelf components may introduce the largest flow restrictions, such as the inner diameter of the Labsmith *cross* or *tee* being 250 μm or the largest inner diameter for a 360 μm OD capillary; the maximum tolerable pressure is also limited to approximately 1,000 psi.

Sample Injection

The central sample line was a continuous 100 μm inner diameter fused silica capillary with a 160 μm outer diameter and a length of 1.5 m (Polymicro, Phoenix, AZ, USA). This capillary directly connected the reservoir with the interaction region, passing through a vacuum feedthrough and then through a microfluidic *Interconnect Cross* (C360–204, LabSmith, Livermore, CA USA; C360–203 *Interconnect Tee* may also be used with no need to plug the fourth channel) (Supplementary Figure 2). Feeding the sample through an uninterrupted straight capillary without filters, unions or connections minimized the risk of sample clogs and leaks, which most often occur at flow channel transitions. In addition, the large capillary

inner diameter allowed the crystal slurry to flow in the system with no inline filtration or filters at the reservoir. The fitting at the top of the *cross* in Supplementary Figure 2 was an adapter fitting (T116-A360 as well as T116–100, LabSmith, Livermore, CA, USA) which compressed a 1/16” (1.6 mm) OD, 0.007” (178 μm) ID polymer (FEP) tubing sleeve (F-238, Upchurch, Oak Harbor, WA, USA) onto the sample capillary. This connection method was necessary to properly seal the capillary to the *cross*. The sheath line at the bottom of the figure was a short 5 cm fused silica capillary with an outer diameter of 360 μm and an inner diameter of 180, 200, or 250 μm depending on the desired flow rate of the sheath liquid possible with the driving pressure available. The length and ID of this line were chosen to allow sufficient flow for the sheath line. This outer capillary was connected to the *cross*, and the sheath liquid was supplied from the third port of the cross (the right port in the figure) through a compatible microfluidic tubing; we typically used silica capillaries with 360 μm outer diameters and 75 or 100 μm inner diameters, depending on flow rate desired. For simplicity, the injector has been designed to operate at relatively low backing pressures (up to a few atmospheres). To achieve a given flow rate of the liquids, the fluidic resistance of the lines is varied, typically by changing the inner diameter of the capillaries used in the injector. For this experiment, the sheath liquid line was connected to a syringe filled with the appropriate sister liquor, driven by a syringe pump (PHD Ultra, 703006, Harvard Apparatus, Holliston, MA, USA). We electrically charged the sheath liquid between 0–5,000 V potential using an in-line conductive charging union (M-572, Upchurch, Oak Harbor, WA, USA) connected to a SRS PS350 (Stanford Research Systems, Sunnyvale, CA, USA) high voltage source.

The capillary assembly was loaded into the CXI 1 × 1 μm^2 focused beam chamber with a custom load lock system developed at Lawrence Berkeley National Laboratory, Supplementary Figures 7 and 8. This load lock system allowed for fast changes and cleaning of the injector capillary without having to vent the main chamber of the CXI instrument. A grounded, conical counter electrode with a 1 cm opening was placed approximately 5 mm below the capillary tip; the capillaries and opening of the cone were coaxial. The angle of the cone and its distance from the tip were set to enable a diffraction cone with a 45° half-angle. All capillaries were fed through vacuum flanges with 1/16” (1.6 mm) Swagelok bulkhead fittings using appropriately sized polymer sleeves. The sheath reservoir was a 1 ml Gastight Hamilton syringe with a PTFE Luer tip (1001 TLL SYR, Hamilton, USA). The sample was supplied either from a 500 μl Hamilton gas tight syringe (for PSII and thermolysin) using a syringe pump or from a custom 5 ml reservoir (for the ribosome crystals) developed at the Sample Environment Group at LCLS. This stainless steel reservoir contains a custom Teflon plug that separates the sample slurry from the pushing fluid (which was either water, or the mother liquor to mitigate problems from any potential leaks) as shown schematically at the top of Figure 1 and in Supplementary Figure 8. The backing fluid is driven by another syringe pump or can be pressurized by compressed gas.

PSII injection improvement in new mother liquor—Previous time-resolved PSII experiments[26–28] carried out at LCLS relied on the single-capillary MESH injector. In previous LCLS solution spectroscopy experiments, the 70 mg/ml protein solution was supplemented with 1.0–1.4 M sucrose to prevent freezing. In SFX experiments, a prior

crystallization condition of 10% (w/v) PEG 2,000 was supplemented with 30% (v/v) glycerol to prevent freezing in vacuum and to reduce sample consumption during injection. Data up to 4.5 Å resolution were collected during these earlier experiments[28], but higher resolution for this sample was desired in order to better observe subtle time-dependent structural changes of the manganese metal center (Mn_4CaO_5) in its photodriven catalytic cycle. An improved crystallization condition yielding higher-quality PSII crystals contained a high percentage of PEG 5,000[12] (30–35% w/v) which caused the meniscus of the MESH to dehydrate quickly in vacuum and fail. These failure modes occurred frequently and limited the data collection time (Supplementary Fig. 4c). The coMESH successfully injected the new mother liquor into vacuum by protecting it with the sister liquor (Supplementary Table 1 and Supplementary Figure 3b,c), thus eliminating the sudden failures caused by dried PEG 5,000 at the meniscus. Supplementary Table 1 lists several representative buffer compositions in which the original, single-capillary MESH configuration failed *in vacuo*, but jetted properly using the new coMESH configurations. Supplementary Figure 5 compares composite maximum images of two representative nine-minute runs of PSII crystal suspensions using the two different coMESH injector setups at the Coherent X-ray Imaging (CXI) instrument[13] of the LCLS. The single-capillary MESH setup, used previously, required the addition of 35 to 40% of ethylene glycol into the improved mother liquor, whereas the coMESH setup eliminated the need for ethylene glycol. The coMESH with a protruded inner capillary was used for thermolysin crystal suspensions (Supplementary Figure 3d) and allowed collection of sufficient diffraction data for obtaining the structure (Supplementary Figure 6). Tests with PSII crystal suspension in this protruded capillary geometry gave no indication of powder rings from dried PEG 5,000 (Supplementary Figure 5a), but there was still indication of freezing of the carrier liquid. In contrast, when using the coMESH with co-terminal capillaries (Supplementary Figure 5b), freezing or drying problems were eliminated and allowed the observation of diffraction beyond 3.0 Å. This decrease in jet failures resulted in continuous run-times of 2–2.5 hours, an improvement over mean runtimes of 20–30 minutes between blockages of the jet in the single-capillary MESH setup.

coMESH for ribosome crystals—The sample reservoir was loaded with 30S ribosome crystal slurry in mother liquor, described above. The sister liquor was identical to the mother liquor in that the original substituent concentrations remained constant with the exception of having a higher MPD concentration of 34% (v/v). The sample capillary was a 100 μm ID × 160 μm OD × 1.5 m long fused silica capillary. The sheath flow capillary was a 75 μm ID × 360 μm OD × 1 m long fused silica capillary. The outer concentric capillary was a 200 μm ID × 360 μm OD × 5 cm long tapered silica capillary. The tips of the inner and outer capillaries were located at the same position. The taper of the outer capillary minimizes the surface on which debris can build up on after X-ray interaction with the sample but is not necessary for operation. The applied voltage on the sheath liquid was typically 3,000 V, and the counter electrode was grounded. The sample ran typically between 0.75–3 μl/min and the sheath flow rate typically matched the sample flow or was slightly faster.

For the study of 30S ribosomal subunit crystals, the inner sample line contained unfiltered crystals in their native mother liquor containing 17% (v/v) 2-methyl-2,4-pentanediol (MPD).

The size distribution of the 30S crystals was uniform (3–10 × 3–10 × 20–30 μm^3) due to their controlled slower growth at 4°C[22]. Occasional larger sized 30S crystals were discarded by repeated gentle differential settling without centrifugation. The outer sister liquor was the same buffer, with no crystals, as the mother liquor in that the original substituent concentrations remained constant while having increased the MPD to 34% (v/v) to aid in vacuum injection. The coMESH injector allowed us to successfully deliver 30S ribosomal subunit crystals (Supplementary Figure 3a) and collect sufficient data to solve a complete ambient-temperature SFX structure, which was previously not attainable at an XFEL[16].

coMESH for PSII crystals—The 250 μl Gastight Hamilton glass syringe was loaded with PSII protein crystals in mother liquor, described above. The sister liquor was 50% (v/v) ethylene glycol, 50 mM TRIS (pH 7.5) and 50 mM ammonium sulfate. The sample capillary was a 100 μm ID × 160 μm OD × 1.5 m long fused silica capillary. The sheath flow capillary was a 75 μm ID × 360 μm OD × 1 m fused silica capillary. The outer concentric capillary was a 200 μm ID × 360 μm OD × 5 cm long tapered fused silica capillary. The tips of the inner and outer capillaries were located at the same position. The sample was charged at the needle of the syringe with applied voltages of typically 7,000 V (PS365, Stanford Research Systems, Sunnyvale, CA, USA), and the counter electrode was grounded. The sample ran typically at flow rates between 0.75–3 μl/min and the sheath flow rate matched the sample flow rate or was faster, to ensure proper isolation of the inner flow. For comparison, microcrystal suspensions were also run using the single-capillary MESH setup.

Protruded coMESH for PSII solution and crystals and thermolysin crystals—The solution X-ray emission spectroscopy experiments performed in vacuum could not handle the increased background noise from the thick (on the order of 10 μm) outer sister liquor layer, however, vacuum protection was still needed. This problem was addressed by slightly modifying the injector geometry, which was similar to the PSII setup described above. The exception was that the sample capillary protruded 1 mm beyond the tip of the outer capillary. In the case of thermolysin, the sister liquor was 50% (v/v) ethylene glycol, 100 mM MES (pH 6.5) and 5 mM $CaCl_2$. The sheath line had a smaller ID of 30 μm to increase the fluidic resistance. Once the sheath line was primed with the sister liquor, the line was capped off and allowed only to slowly trickle into vacuum, rather than having a driven flow. The voltage was applied on the sample line, using a metal charging union.

Data Collection and Analysis

Diffraction data collection of 30S ribosomal subunit microcrystals—The SFX experiments with 30S ribosome microcrystals were carried out at the LCLS beamtime ID: CXIG7014 at the SLAC National Accelerator Laboratory (Menlo Park, CA). The LCLS X-ray beam with a pulse duration of 50 fs was focused using X-ray optics in a Kirkpatrick-Baez geometry to a beam size of 1.3 × 1.3 μm^2 full width at half maximum (FWHM) at a pulse energy of 2.9 mJ, a photon energy of 9.5 keV (1.29 Å) and a repetition rate of 120 Hz.

A total of 866,358 detector frames were collected with the Cornell-SLAC Pixel Array Detector (CSPAD)[29] corresponding to 120 min of data collection. The total beamtime needed for this dataset was 144 minutes, which shows the efficiency of this injector system,

as due to lack of blockages no dead time was accumulated. Individual diffraction pattern hits were defined as frames containing more than 30 Bragg peaks with a minimum signal-to-noise ratio larger than 4.5 which were a total of 44,106 images corresponding to an average hit rate of 5.1%. The detector distance was set to 223 mm, with an achievable resolution of 3.08 Å at the edge of the detector (2.6 Å in the corner). In this experiment, the fourth quadrant of the CSPAD detector was damaged and did not collect data.

After the detection of hits and following the conversion of individual diffraction patterns to the HDF5 format, the software suite *CrystFEL*[30] (version 0.5.4, git ID: 0477328) was used for crystallographic analysis. The peak location information from *CHEETAH*[31] was used for the indexing of individual, randomly oriented crystal diffraction patterns using FFT-based indexing approaches. The detector geometry was refined using an automated algorithm to match found and predicted peaks to subpixel accuracy (Yefanov *et al.* in press). The integration step was performed using a built-in Monte-Carlo algorithm[32, 33] to estimate accurate structure factors from thousands of individually measured Bragg peaks. After the application of per pattern resolution cutoff, frames that didn't match to an initial merged dataset with a Pearson correlation coefficient of greater than 0.4, were excluded from the final dataset. The final set of indexed patterns, containing 20667 frames (47% indexing rate), was merged into a final dataset (Overall CC* = 0.9822; 3.4 Å cutoff) for further analysis ($P4_12_12$, unit cell: a = b = 401.3 Å, c = 176.4 Å; $\alpha = \beta = \gamma = 90°$). The final resolution cutoff was estimated to be 3.4 Å using a combination of *CC**[34] and other refinement parameters. The final dataset had overall R_{split} = 29.42 %, and *CC** = 0.70 in the highest resolution shell.

Diffraction data collection of PSII and thermolysin microcrystals—The SFX experiments with PSII and thermolysin microcrystals were carried out at the LCLS (beamtime ID: CXIG3614) at SLAC. The LCLS X-ray beam with a pulse duration of 50 fs was focused using X-ray optics in a Kirkpatrick-Baez geometry to a beam size of 1.3 × 1.3 μm^2 FWHM at a pulse energy of 0.9 mJ, using a photon energy of 7.1 keV (1.74 Å) and a repetition rate of 120 Hz. Diffraction data were analyzed using the *cctbx.xfel* software package[6, 35]. The maximum intensity composite images were generated by adding all indexable diffraction patterns of one run (about 9 minutes of measurement time). For thermolysin, 153,943 CSPAD images were recorded during 21.5 min of data collection. Frames containing at least 16 Bragg peaks with a minimum ADU value of 450 and at least 4 pixels in total size were considered hits, giving a total of 71,519 frames, and a 46.5% hit rate. The detector distance was set to 119 mm, with an achievable resolution of 2.7 Å at the edge of the detector (2.2 Å in the corner). 38,222 hits were indexed in *cctbx.xfel* using FFT-based indexing approaches (53.4% indexing rate). The detector geometry was refined using an automated algorithm to match found and predicted peaks to subpixel accuracy[6]. Filters were applied that excluded frames whose partial Bragg spot intensity measurements failed to match a reference set of full measurements with a Pearson correlation coefficient of at least 0.1. Frames were also excluded if they indexed in the wrong Bravais group, had outlying unit cell dimensions, or had very low signal, leaving 37,487 frames in the final dataset. This set of indexed patterns was postrefined and merged into a final dataset[35] (overall CC* =94.0%; 2.25 Å cutoff) for further analysis ($P6_122$, unit cell: a = b = 93.8 Å, c = 132.2 Å; $\alpha = \beta = 90°$, $\gamma = 120°$). The resolution cutoff was estimated to be 2.25 Å using a combination

of *CC**[34] and other refinement parameters. The final dataset had overall R_{split} = 9.4%, and *CC** = 0.16 in the highest resolution shell.

30S Ribosomal Subunit Structure refinement

We determined the ambient temperature 30S-paromomycin structure using the automated molecular replacement program *Phaser*[36] with the previously published cryo-cooled 30S ribosomal subunit-paromomycin complex synchrotron structure as a search model (PDB entry 4DR2)[14]. The resulting structure was refined with rRNA modifications, which are mostly located near the decoding center at which paromomycin binds. This choice of starting search model minimized experimental variations between the two structures such as sample preparation, crystal growth, model registry and data processing. Coordinates of the 4DR2 with additional RNA and protein modifications were used for initial rigid body refinement with the *PHENIX*[37] software package. During initial refinement of ambient temperature XFEL structure, the entire 16S rRNA h28 “hinge 1” region was omitted and the new h28 model was built into unbiased difference density using *RCrane*[38]. After simulated-annealing refinement, individual coordinates, three group B factors per residue, and TLS parameters were refined. Potential positions of magnesium or potassium ions were compared with those in a high-resolution (2.5 Å) 30S subunit structure (PDB accession code 2VQE)[39] in program *COOT*[40], and positions with strong difference density were retained. All magnesium atoms were replaced with magnesium hexahydrate. Water molecules located outside of significant electron density were manually removed. The Ramachandran statistics (most favored/additionally allowed/generously allowed/disallowed) are 90.4/8.2/1.3/0.1% respectively. The structure refinement statistics are summarized in Supplementary Table 2. Structure alignments were performed using the alignment algorithm of *PyMOL* (www.schrodinger.com/pymol) with the default 2σ rejection criterion and five iterative alignment cycles. Alignments used to detect repositioning of the 30S subunit helix 28 in both crystal structures were performed using 16S rRNA phosphate atoms from residues 5–1,532. All X-ray crystal structure figures were produced with *PyMOL*.

Thermolysin Structure refinement

We determined the thermolysin structure using the program *Phaser*[36] by using the previously published SFX structure as a search model (PDB entry 4OW3)[6]. Coordinates of the 4OW3 entry were used for initial rigid body refinement with the *PHENIX*[37] software package followed by individual coordinates, three group B factors per residue, and TLS parameter refinement. Potential positions of water molecules were compared with those in a high-resolution (1.8 Å) thermolysin SFX structure (PDB accession code 4TNL)[28] in program *COOT*[40], and positions with strong difference density were retained. The Ramachandran statistics (most favored/additionally allowed/generously allowed/disallowed) are 93.0/5.9/1.1/0.0% respectively. The structure refinement statistics are summarized in Supplementary Table 2. All X-ray crystal structure figures were produced with *PyMOL*.

Supplementary Material

Refer to Web version on PubMed Central for supplementary material.

Acknowledgments

Portions of this research were carried out at the Linac Coherent Light Source (LCLS) at the SLAC National Accelerator Laboratory. LCLS is supported by the U.S. Department of Energy (DOE), Office of Science, Office of Basic Energy Sciences (OBES) under Contract No. DE-AC02-76SF00515. This research used resources of the National Energy Research Scientific Computing Center, a DOE Office of Science User Facility supported by the Office of Science, DOE, under Contract No. DE-AC02-05CH11231. JY and VKY are supported by Office of Science, OBES, Chemical Sciences, Geosciences, and Biosciences CSGB of the DOE under Contract No. DE-AC02-05CH11231 for X-ray methodology and instrumentation. The LCLS is acknowledged for beam time access under experiment no. cxig7014, cxib6714 and cxig3614. EHD, HL, RGS, MJB, CYH and HD acknowledge the support of the OBES through the AMOS program within the CSGB and the DOE through the SLAC Laboratory Directed Research and Development Program. NKS acknowledges an LBNL Laboratory Directed Research and Development award under Contract No. DE-AC02-05CH11231. EHD acknowledges financial support from the Stanford University Dean of Research. HD, SMS and JDP acknowledge support from the joint Stanford ChEM-H and SLAC National Accelerator Laboratory seed grant program. This work is supported by National Institute of Health (NIH) grants GM51266 (JDP), GM082545 (EVP), GM055302 (VKY), GM110501 (JY) GM095887 and GM102520 (NKS). The DFG-Cluster of Excellence “UniCat” coordinated by the Technische Universitaet at Berlin and Sfb1078, TP A5 (AZ, MI); and the Human Frontiers Science Project Award No. RGP0005/2011 (HL) and RGP0063/2013 310 (JY and AZ). CG kindly thanks the PIER Helmholtz Graduate School, as well as the Helmholtz Association for financial support. HD acknowledges valuable discussions with A. Takeuchi, K. Dursuncan and E. Satunaz. We thank M. West for support in designing and machining the injector load lock setup and G. Stewart for excellent technical assistance with creating the graphics for Figure 1.

References

1. Neutze R, Wouts R, van der Spoel D, Weckert E, Hajdu J. Nature. 2000; 406:752–757. [PubMed: 10963603]
2. Tenboer J, et al. Science. 2014; 346:1242–1246. [PubMed: 25477465]
3. Chapman HN, et al. Nature. 2011; 470:73–77. [PubMed: 21293373]
4. Liu W, et al. Science. 2013; 342:1521–1524. [PubMed: 24357322]
5. Boutet S, et al. Science. 2012; 337:362–364. [PubMed: 22653729]
6. Hattne J, et al. Nat Methods. 2014; 11:545–548. [PubMed: 24633409]
7. Hunter MS, et al. Sci Rep. 2014; 4:6026. [PubMed: 25113598]
8. DePonte DP, et al. Micron. 2009; 40:507–509. [PubMed: 19246201]
9. Sierra RG, et al. Acta Crystallogr D Biol Crystallogr. 2012; 68:1584–1587. [PubMed: 23090408]
10. Weierstall U, et al. Nat Commun. 2014; 5:3309. [PubMed: 24525480]
11. Sugahara M, et al. Nat Methods. 2015; 12:61–63. [PubMed: 25384243]
12. Hellmich J, et al. Structure. 2014; 22:1607–1615. [PubMed: 25438669]
13. Liang M, et al. J Synchrotron Radiat. 2015; 22:514–519. [PubMed: 25931062]
14. Demirci H, et al. Nat Commun. 2013; 4:1355. [PubMed: 23322043]
15. Wilson DJ, Konermann L. Anal Chem. 2003; 75:6408–6414. [PubMed: 16465695]
16. Demirci H, et al. Acta Crystallogr Sect F Struct Biol Cryst Commun. 2013; 69:1066–1069.
17. Petrov A, Chen J, O’Leary S, Tsai A, Puglisi JD. Cold Spring Harb Perspect Biol. 2012; 4:a011551. [PubMed: 22798542]
18. Warkentin M, Hopkins JB, Haber JB, Blaha G, Thorne RE. Acta Crystallogr D Biol Crystallogr. 2014; 70:2890–2896. [PubMed: 25372680]
19. Mohan S, Donohue JP, Noller HF. Proc Natl Acad Sci U S A. 2014; 111:13325–13330. [PubMed: 25187561]
20. Suga M, et al. Nature. 2015; 517:99–103. [PubMed: 25470056]
21. Oshima T, Imahori K. J Biochem. 1974; 75:179–183. [PubMed: 4601162]
22. Demirci H, et al. RNA. 2010; 16:2319–2324. [PubMed: 20962038]
23. Wimberly BT, et al. Nature. 2000; 407:327–339. [PubMed: 11014182]
24. Ibrahim M, et al. Structural Dynamics. 2015; 2
25. Kern J, et al. Biochim Biophys Acta. 2005; 1706:147–157. [PubMed: 15620375]
26. Kern J, et al. Proc Natl Acad Sci U S A. 2012; 109:9721–9726. [PubMed: 22665786]

27. Kern J, et al. Science. 2013; 340:491–495. [PubMed: 23413188]
28. Kern J, et al. Nat Commun. 2014; 5:4371. [PubMed: 25006873]
29. Hart P, et al. Proc of SPIE. 2012; 8504:85040C.
30. White TA, et al. Journal of Applied Crystallography. 2012; 45:335–341.
31. Barty A, et al. J Appl Crystallogr. 2014; 47:1118–1131. [PubMed: 24904246]
32. Kirian RA, et al. Optics Express. 2010; 18:5713–5723. [PubMed: 20389587]
33. White TA, et al. Acta Crystallogr D Biol Crystallogr. 2013; 69:1231–1240. [PubMed: 23793149]
34. Karplus PA, Diederichs K. Science. 2012; 336:1030–1033. [PubMed: 22628654]
35. Sauter NK. J Synchrotron Radiat. 2015; 22:239–248. [PubMed: 25723925]
36. McCoy AJ, et al. J Appl Crystallogr. 2007; 40:658–674. [PubMed: 19461840]
37. Adams PD, et al. Acta Crystallogr D Biol Crystallogr. 2010; 66:213–221. [PubMed: 20124702]
38. Keating KS, Pyle AM. Acta Crystallogr D Biol Crystallogr. 2012; 68:985–995. [PubMed: 22868764]
39. Kurata S, et al. J Biol Chem. 2008; 283:18801–18811. [PubMed: 18456657]
40. Emsley P, Lohkamp B, Scott WG, Cowtan K. Acta Crystallogr D Biol Crystallogr. 2010; 66:486–501. [PubMed: 20383002]

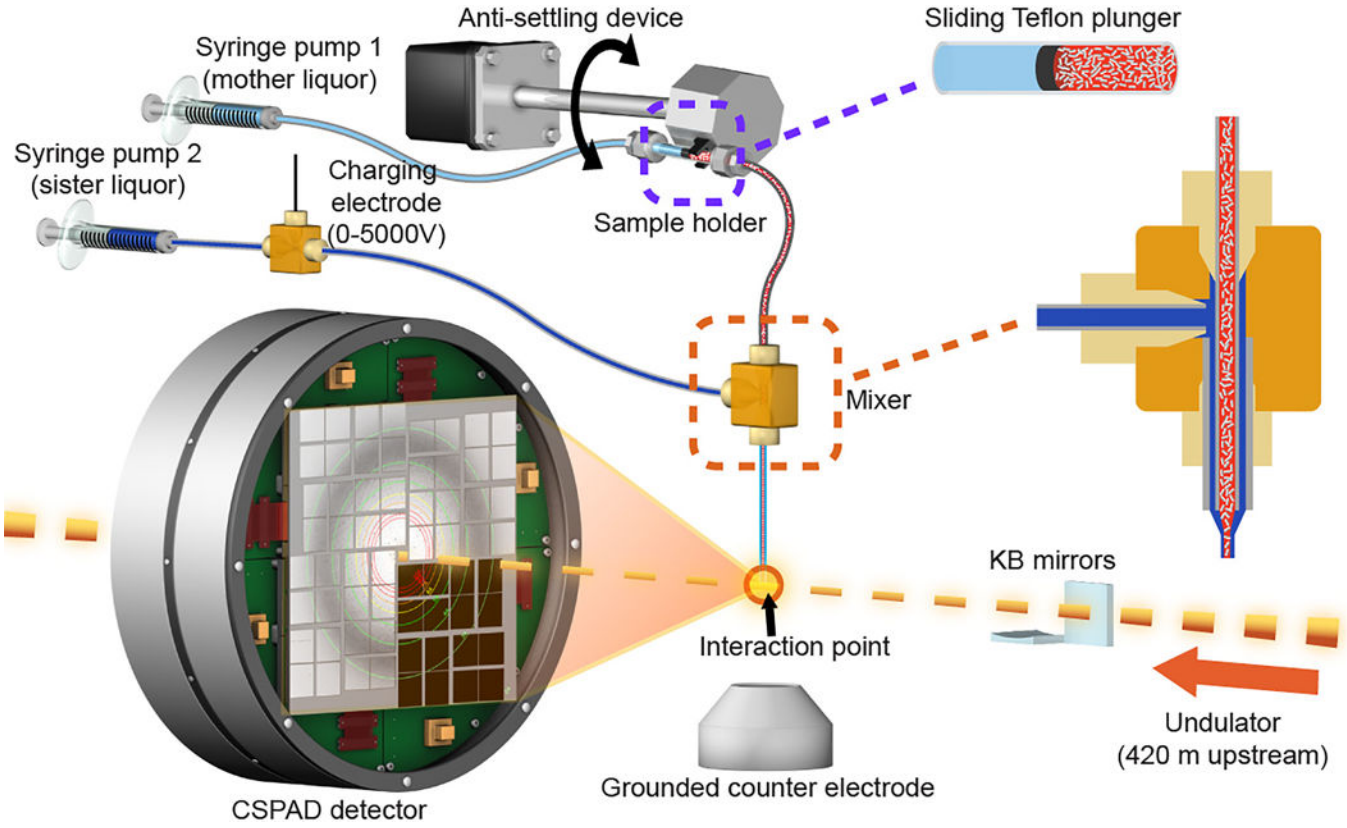

Figure 1.

Diagram of the concentric-flow MESH injector setup at the CXI instrument of the LCLS. The liquid jet, comprising ribosome microcrystals and their mother liquor (17% v/v MPD; colored in red), flowed in the continuous inner capillary (100 μm × 160 μm × 1.5 m; colored in gray) (Supplementary Fig. 3a). The sister liquor containing 34% MPD (colored in dark blue) was charged by a high voltage power supply (0–5,000 V) for electro-focusing of the liquid jet. A mixer (indicated within the dashed orange rectangle) joined the two capillaries (colored in gray) concentrically (Supplementary Fig. 2). The sample reservoir had a Teflon plunger (colored in black) which separated the sample reservoir from the driving fluid (colored in light blue). The reservoir was mounted on an anti-settling device which rotated, at an angle, about the capillary axis to keep the protein crystals suspended homogenously in the slurry. The liquid jet and the LCLS pulses interacted at the point indicated by the orange circle. The bottom right quadrant of the detector was non-functional during ribosome data collection and is shown in black.

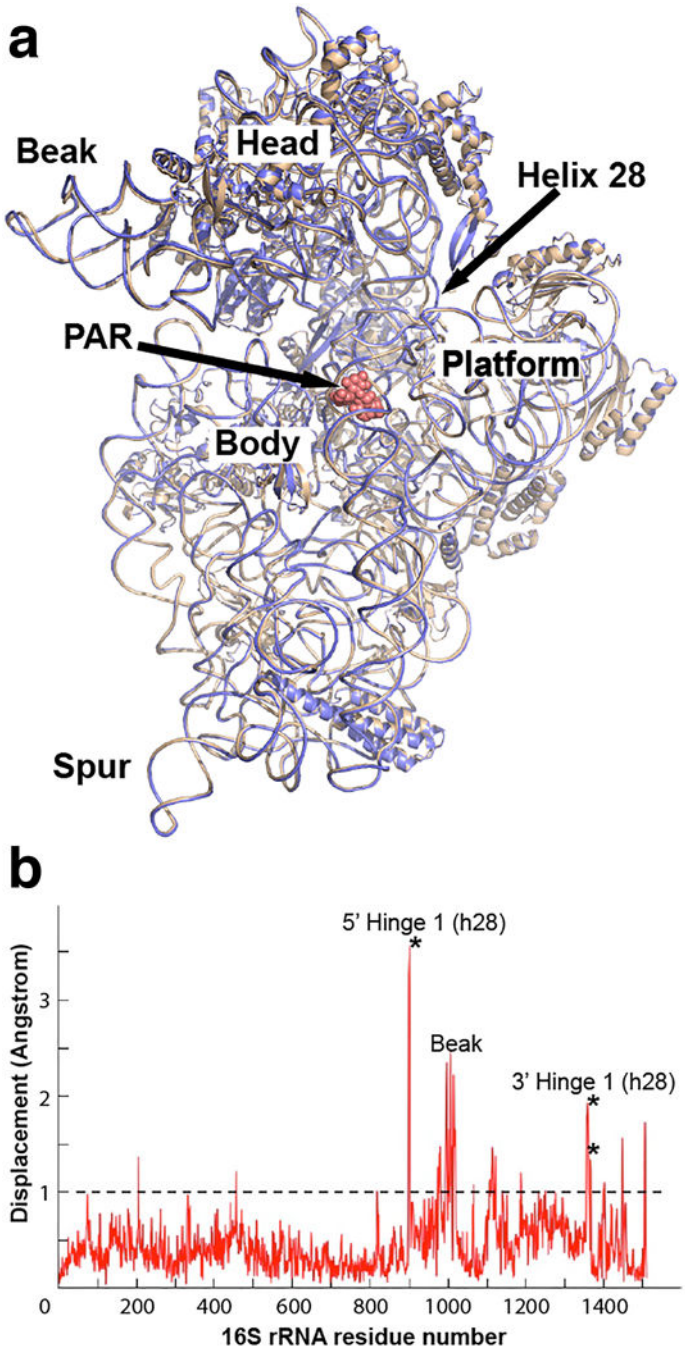

Figure 2.

Comparison of cryo-cooled and ambient temperature 30S-paromomycin complex structures. (**a**) The crystal structures of the *T. thermophilus* 30S subunits collected at both temperatures are shown. The ambient-temperature structure (colored in wheat) is superposed on the cryo structure (colored in blue). The positions of the major 30S domains are indicated with text on the structure. The location of paromomycin (PAR) (salmon-colored spheres) within the ambient temperature structure as well as 16S rRNA helix 28 (h28) are shown by arrows. All X-ray crystal structure figures were produced with PyMOL (www.schrodinger.com/pymol)

(**b**) Pairwise distances between 16S rRNA phosphate atoms were plotted after aligning all phosphate atoms of bases 5–1532 between the ambient and cryo 30S structures. Major shifts above 1 Å can be seen as sharp spikes and observed at and around the hinge1 region of helix28 (indicated by the asterisks) and beak domain. The dotted line denotes a 1 Å displacement threshold.

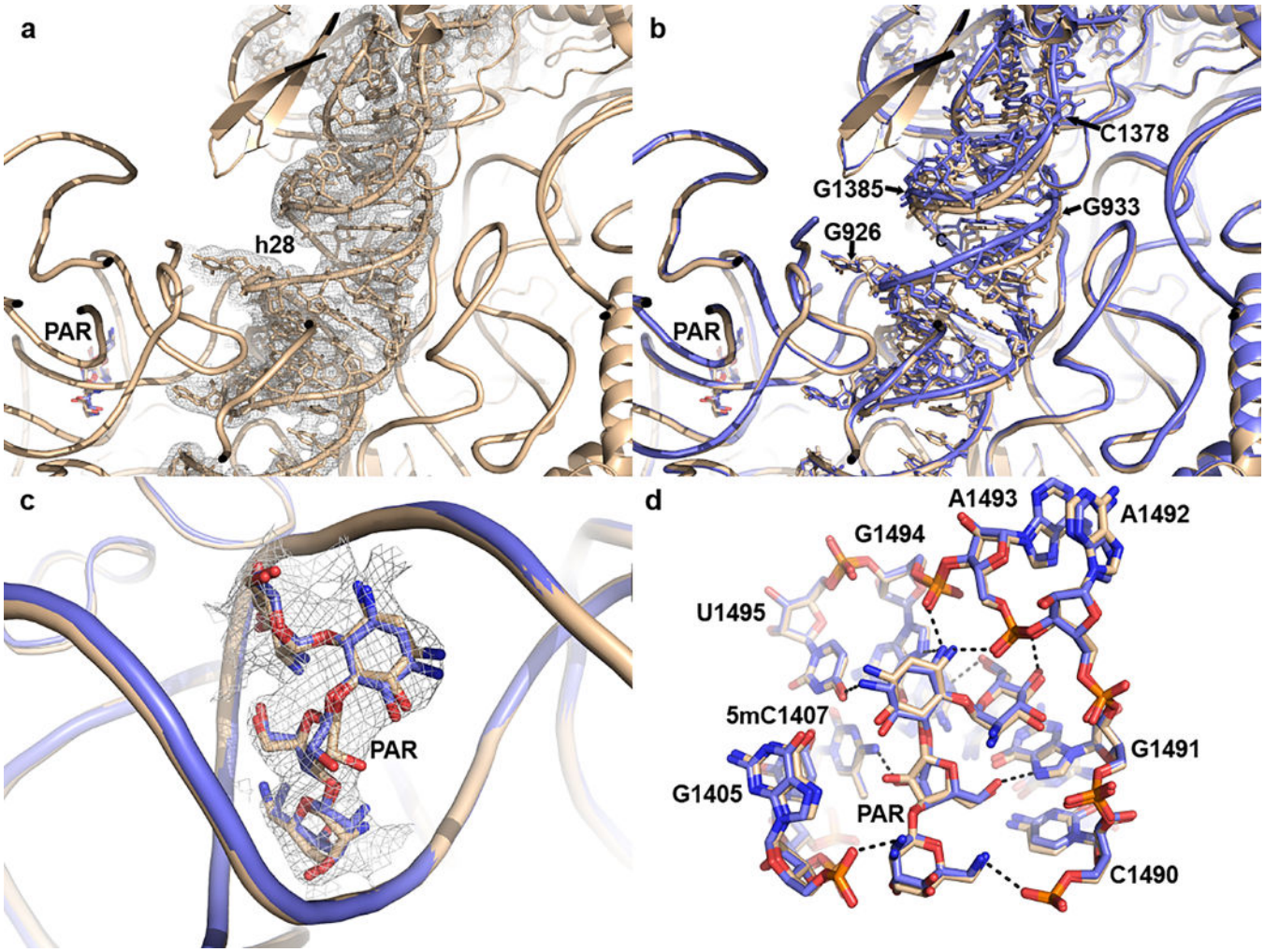

Figure 3.

Structural changes were observed in helix28 and in the paromomycin binding at ambient temperature. (**a**) Final unbiased F_o-F_c simple omit electron density map of h28 contoured at 3σ level, colored in gray and shown at 3 Å. The color scheme is the same as in Fig. 2. The locations of the paromomycin and h28 are indicated. (**b**) Superposition of the cryo- and ambient-temperature structures revealed displacement of the h28 backbone. This view illustrates the shifts in positions 926–933 and 1,375–1,385. (**c**) Final unbiased F_o-F_c simple omit difference electron density map of paromomycin binding site contoured at 3σ level, colored in gray and shown at 3 Å. (**d**) Comparison of the contacts between cryo- and ambient temperature 16S rRNA helix 44 (h44) and paromomycin. The bending of the paromomycin molecule is visible with altered H-bonding network, view in (c) rotated around vertical y-axis nearly 180°.